Report for the Joint Use/Research of the Institute for Planetary Materials, Okayama University

2022 fiscal year first term / second term / others

30/4/2023

Category: International Joint Research/ General Joint Research/ Joint Use of Facility/ Workshop

Name of the research project: Influence of oxygen fugacity on depth variation of olivine-wadsleyite phase transformation: Implication for 410-km discontinuity depth anomaly

Principal applicant: Chengcheng Zhao

Affiliated institution and department: Zhejiang University

Collaborator

Name: Professor Takashi Yoshino

Affiliated institution and department: Institute for Planetary Materials

Research report:

1) Please write the research report with free format, but include followings: research purpose, actually conducted research, and research outcomes. If necessary, you can add another pages.
2) For the workshop, please write the report for the workshop. Also, attach the program, abstracts, and list of the participants etc.
3) Please add Collaborator's Name, Affiliated institution and department as needed.

To determine the exact depth (pressure) of olivine to wadsleyite transformation, synchrotron experiment is required. So my research project changed to determining redox kinetics of hydrous olivine at high pressure. Below is the detailed research report.

Research project: Redox kinetics of hydrous olivine at high pressure and its implication on redox exchange between subducting slab and the surrounding upper mantle

Research purpose:

1. Determine redox kinetics of hydrous olivine at high pressure from 4 to 12 GPa;
2. Figure out the redox mechanism of hydrous olivine at high pressure;
3. Calculate the possible influence on redox budget of subducting slab with pressure.

Experimental procedures:

1. Preparation of starting materials

Reactant grade MgO, SiO_2, Fe_2O_3 powder of stoichiometric forsterite composition were mixed, with 3 wt% additional SiO_2 added as silica buffer. The well-mixed powder was made into pellets of

~ 0.5 mm thickness, which were then baked in a gas mixture furnace at 1300 ºC and either FMQ/RRO or IW buffered conditions for 4 hours. Then the olivine pellets were ground into powder and 5 wt% Pt powder was added as oxygen sensor to monitor oxygen fugacity in-situ. After fully mixing in alcohol, the Pt-doped olivine powder was made into 0.5 mm thick pellets again and baked in the gas mixture furnace at the same temperature and oxygen fugacity conditions as before for another 4 hours. Finally, Pt-doped FMQ/RRO and IW buffered olivine powders were obtained as the starting materials.

2. Synthesis of olivine aggregates and sample characterization

FMQ/RRO and IW buffered olivine powders were loaded into Ni and Mo capsules with ~ 3 mm diameter and ~ 4 mm length respectively, which were inserted into MgO sleeve, graphite/$LaCrO_3$ heater, ZrO_2 insulator and 14 mm octahedron in a sequence (Figs. 1a and 1b). WRe_3 and WRe_{25} thermocouple was set in the middle of the sample capsule to monitor temperature. Before compression, the whole cell assembly was kept in 200 ºC vacuum furnace overnight to minimize absorbed water. 32 mm anvils with 8 mm truncations was later adopted as the second stage in a multi-anvil apparatus. Sintering experiments were conducted from 4 to 12 GPa. After reached the target pressure, temperature was increased to 1200 ºC at a rate of ~ 100 ºC/min. 1-2 hours was adopted to get well sintered olivine aggregate. The detailed experimental conditions are summarized in Table 1.

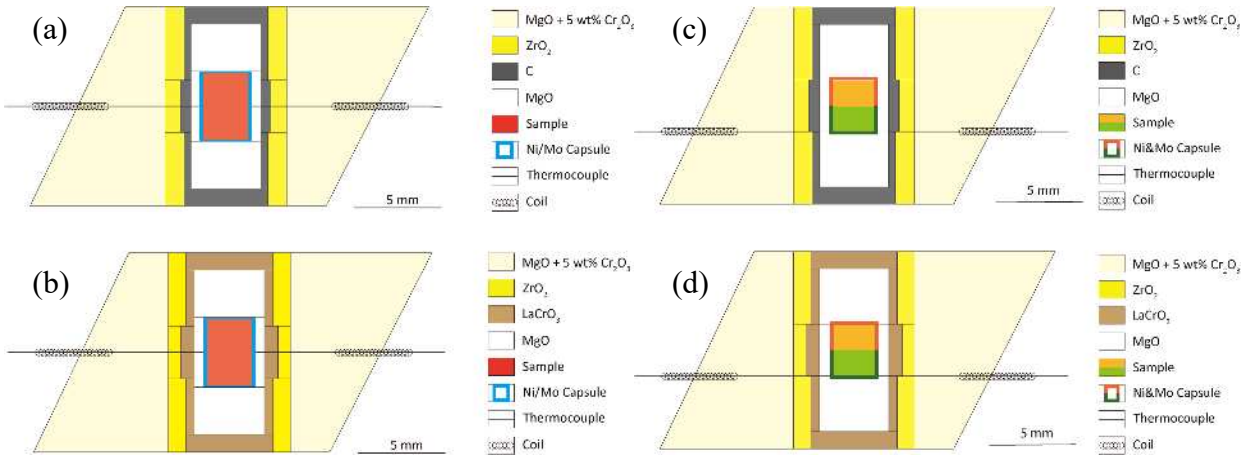

Fig. 1 14/8 cell assembly for synthesis and diffusion experiment. (a) (b) Sintering experiment configuration at 4-8 and 12 GPa respectively. (c) (d) Diffusion experiment configuration

After recovery, micro-texture was observed by scanning electron microscope (SEM). Average grain size of olivine was measured to be 3–9 μm, using intercept method (Mendelson, 1969) with the relation d = cL where d is grain size, L is length of intercept, and c is a constant of 1.56. Chemical composition of ~ 20 points of Pt alloys and neighboring olivine grain was measured by electron microprobe (EPMA) from near Ni/Mo capsule to the center on the cross section of sample. The almost constant oxygen fugacity distribution for samples at 4 and 8 GPa (Fig. 2 and Table 1) calculated from method described in Faul et al. (2017) indicates that a new redox state has been

achieved across the sample. However, sample at 12 GPa shows a little bit higher standard deviation from constant oxygen fugacity.

Table 1 Synthesis experiment summary using multi-anvil apparatus

Run No.	Starting material	Capsule	P (GPa)	T (ºC)	Duration (h)	fO_2	fO_2 (ΔFMQ)	fO_2 (ΔIW)	Grain size (μm)	H_2O* (ppm)
5K3769	Ol+3wt%SiO_2+5wt%Pt (FMQ)	Ni foil	4	1200	1	-7.4(0.1)	-1.5(0.1)	3.0(0.1)	6.3(3.5)	140(20)
5K3770	Ol+3wt%SiO_2+5wt%Pt (IW)	Mo foil				-9.5(0.1)	-3.7(0.1)	0.9(0.1)	3.4(1.8)	80(10)
5K3780	Ol+3wt%SiO_2+5wt%Pt (RRO)	Ni foil	8	1200	1	-3.5(0.2)	-0.2(0.2)	5.4(0.2)	8.3(4.5)	/
1K3583	Ol+3wt%SiO_2+5wt%Pt (IW)	Mo foil				-7.5(0.1)	-4.1(0.1)	1.5(0.1)	5.9(3.0)	/
5K3787	Ol+3wt%SiO_2+5wt%Pt (RRO)	Ni foil	12	1200	1	-1.1(0.4)	-0.4(0.4)	6.3(0.4)	8.4(4.1)	/
1K3589	Ol+3wt%SiO_2+5wt%Pt (IW)	Mo foil			2	-5.8(0.3)	-5.0(0.3)	1.7(0.3)	6.1(2.9)	/

Number in parenthesis is the standard deviation error.

* "/" in water content column means water content was not measured.

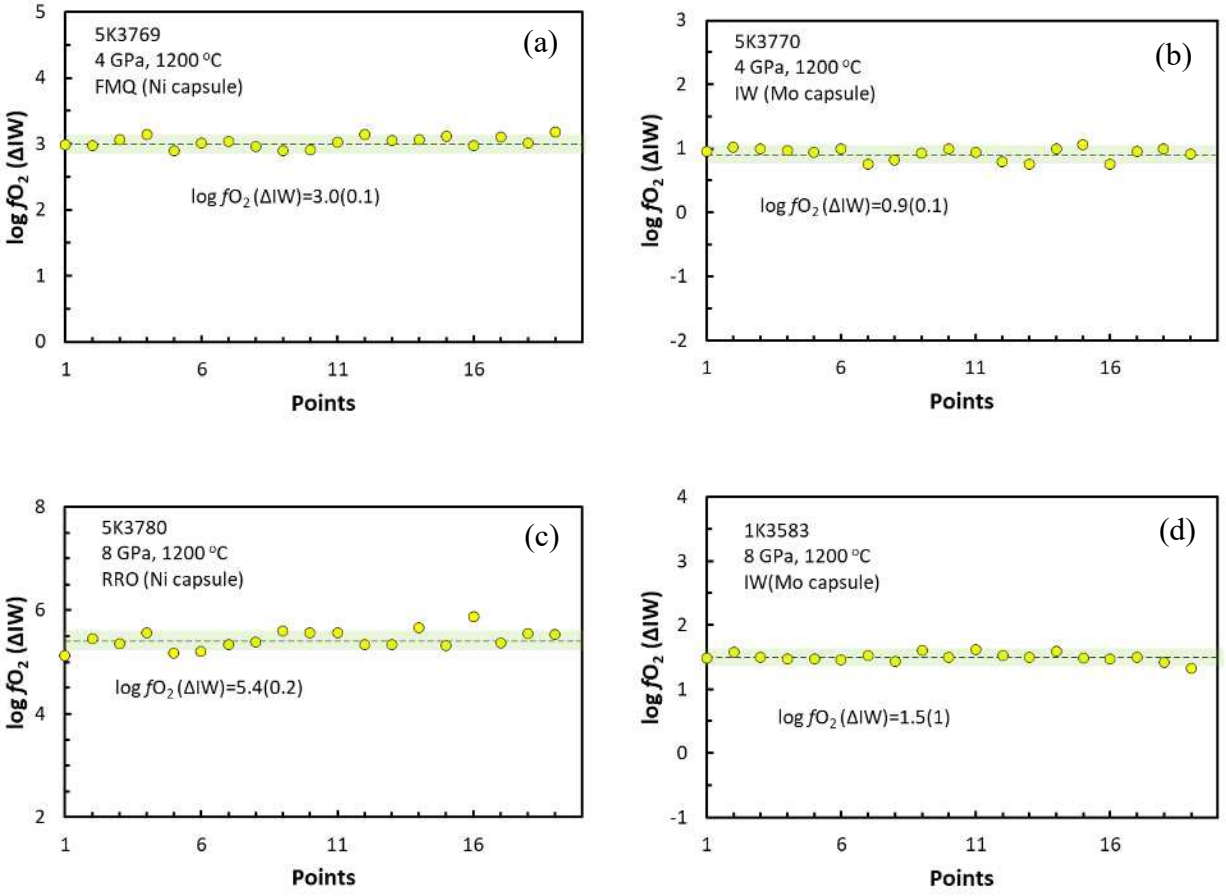

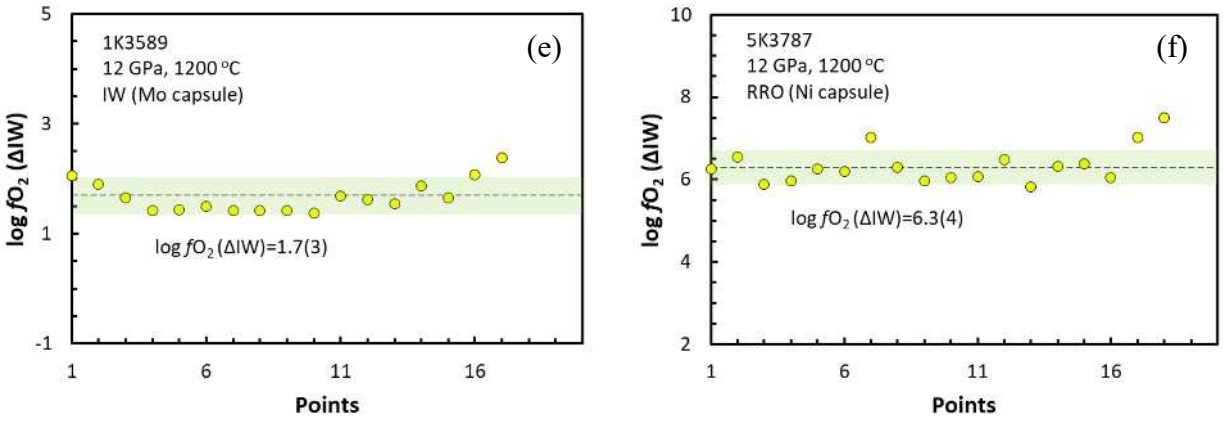

Fig. 2 Oxygen fugacity distribution of the starting olivine aggregate at different pressures

3. Redox experiment and sample characterization

The recovered olivine aggregate was cut into two pieces of 1-1.5 mm thickness from the middle perpendicular to the longitudinal direction. One FMQ/RRO buffered piece was stacked on one IW buffered piece sintered at the same pressure and temperature condition to form a redox couple, with contact interfaces of the two redox parts carefully polished to ensure good contact. The original Ni and Mo capsules for both parts were retained. The redox couple was inserted into a MgO sleeve, graphite/$LaCrO_3$ heater, ZrO_2 insulator and 14 mm octahedron in a sequence (Figs. 1c and 1d). WRe_3 and WRe_{25} thermocouple was set in the bottom of the redox capsule to monitor temperature.32 mm anvil with 8 mm truncation was used.

Redox experiment was performed at the same pressure and temperature with that for sintering experiment to minimize possible interference from re-equilibrating of oxygen fugacity. When target pressure was achieved, temperature was increased to 1200 °C at a rate of ~ 100 °C/min. Different durations were adopted at different pressures in order to get oxygen fugacity profile. Detailed experimental conditions are summarized in Table 2.

Table 2 Experimental summary for redox experiment using multi-anvil apparatus

Run No.	Starting sample	P (GPa)	T (°C)	Duration (h)	Grain size (μm)	Increase (%)	H_2O (ppm)	log D (m^2/s)	Comment
5K3778	5K3769+5K3770	4	1200	3	O: 9.1(5.0)	44	50(10)	-11.78	
					R: 5.3(2.6)	56	30(10)	-11.86	
5K3783	5K3780+1K3583	8	1200	4	O: 11.7(6.5)	41	140(10)	-11.24#	diffuse out
					R: 8.0(3.9)	36	70(10)	-11.67	
5K3788	5K3780+1K3583	8	1200	2	O: 9.5(5.2)	14	180(10)	-11.79#	fO_2 dropped
					R: 6.3(3.1)	7	50(10)	-11.79	
5K3791	5K3787+1K3589	12	1200	1	O: /	/	/	/	
					R: /	/	/	/	

indicate the value is not robust.

After recovery, redox couple was cut into two halves at center, perpendicular to the initial contact interface. One half was double polished to ~ 100 μm thickness for infrared (IR) spectroscopy measurement. A JASCO IRT5200IMPY Fourier-transform IR (FTIR) spectrometer with an aligned transmission geometry was used with an aperture size of 100 × 100 and accumulation scans of 256. 5–10 different points were measured for each redox part. After corrected baseline and normalized thickness, water content was obtained by calibrating IR spectra according to Paterson's method (Paterson, 1982) with an integration range of 3,000–3,730 cm^{-1} and an orientation factor of 1/2. Water content before redox experiment is also acquired for samples synthesized at 4 GPa, while that for sample at 8 GPa is absent. Water content calibrated by other methods are also summarized in Table 3 for comparison. Typical IR spectra are presented in Fig. 3.

The other half of the redox couple was used for SEM and EPMA measurement. A homogeneous texture with average grain size of 5–9 μm was observed (Table 2), with grain growth within 60% for both FMQ/RRO and IW parts. Usually the initial interface was identified as parallel to the juncture between Ni and Mo capsule (Fig. 3). In one couple whose initial interface is tilted, the back scattered electron under SEM provided clear boundary between the two parts (Fig. 4). Chemical composition of Pt particle and neighboring olivine grain were analyzed in the center part of cross section from one to the other end across the redox couple. fO_2 profile as a function of distance from the initial contact interface is plotted (Fig. 5). Redox profile at 4 GPa forms a complete diffusion profile, while those at 8 GPa either diffuse out or has significant drop of oxygen fugacity at the oxidized part.

Table 3 Water content using various calibration methods

Run No.	Redox state	Paterson	Bell/3	Aubaud	Withers
5K3769	FMQ	140(20)	230(40)	190(30)	140(20)
5K3770	IW	80(10)	140(20)	110(20)	90(10)
5K3778	FMQ	50(10)	80(20)	60(10)	50(10)
	IW	30(10)	50(20)	40(10)	30(10)
5K3783	RRO	140(5)	200(10)	160(5)	120(5)
	IW	70(10)	100(10)	90(10)	70(10)
5K3788	RRO	180(10)	260(10)	210(10)	160(10)
	IW	50(5)	80(10)	65(5)	50(5)
5K3791*	RRO	-	-	-	-
	IW	-	-	-	-

* "-" means water content is not measured.

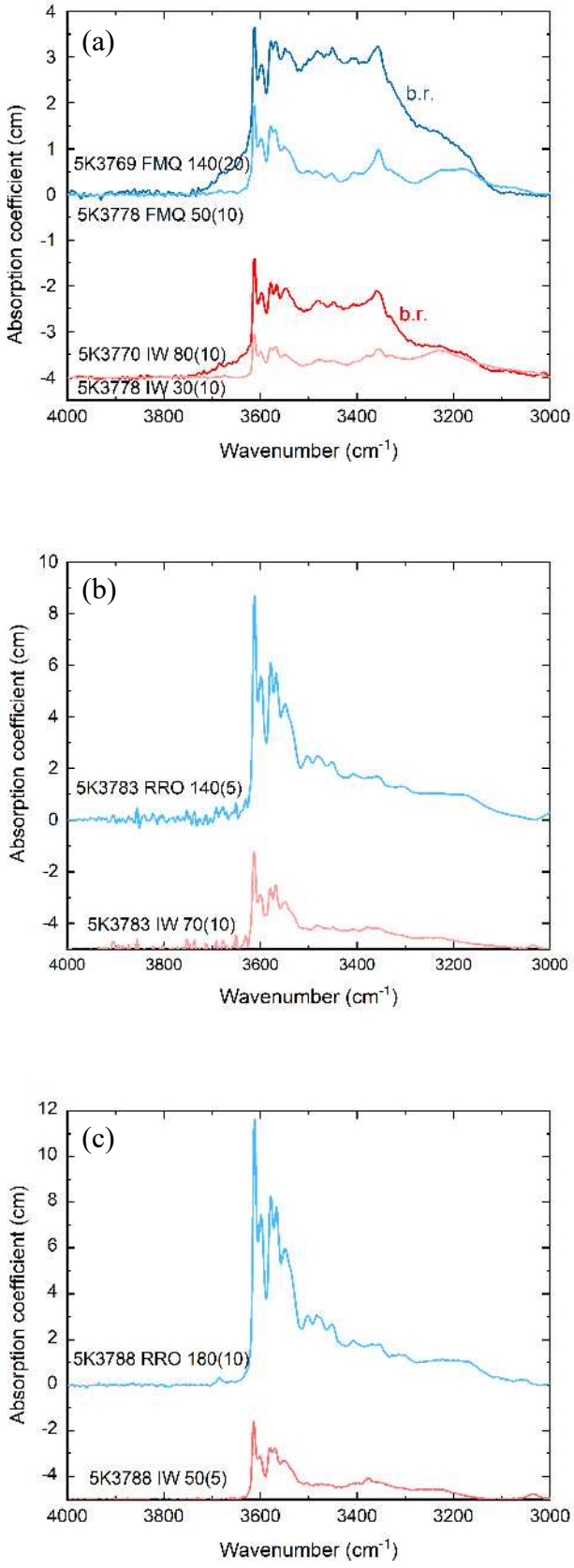

Fig. 3 Typical IR spectra of redox couple before and after redox experiment. "b.r." means water content before redox experiment. Water content before redox experiment at 8 GPa is not measured.

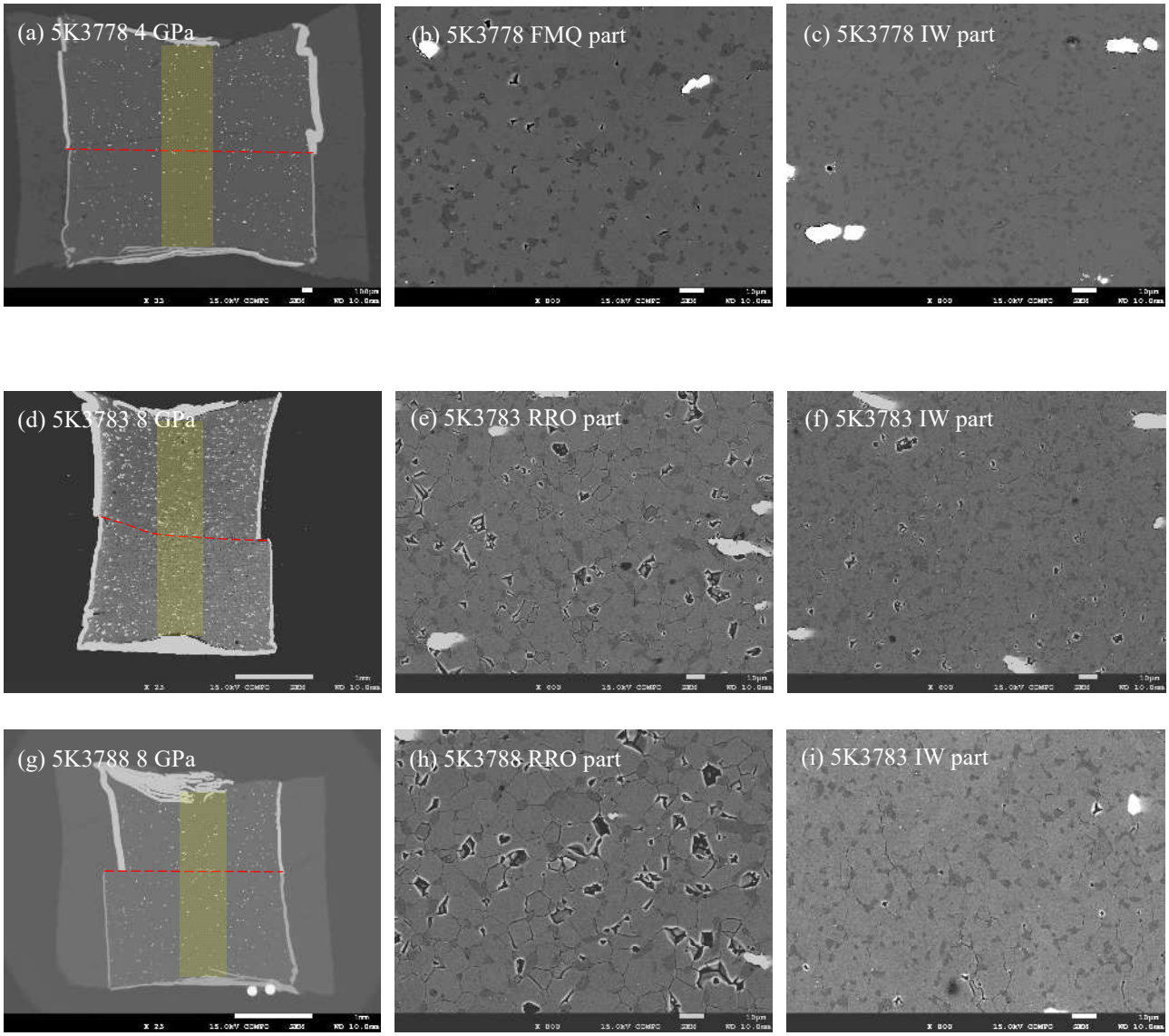

Fig. 4 Sample texture after redox experiment at 4 and 8 GPa. Red dashed lines are the initial contact interfaces of redox couples. Yellowish rectangles are EPMA measurement region, from where oxygen fugacity profiles are obtained. The grey matrix is olivine, while the dark grey grains are pyroxene. Holes without grains appears as black spots.

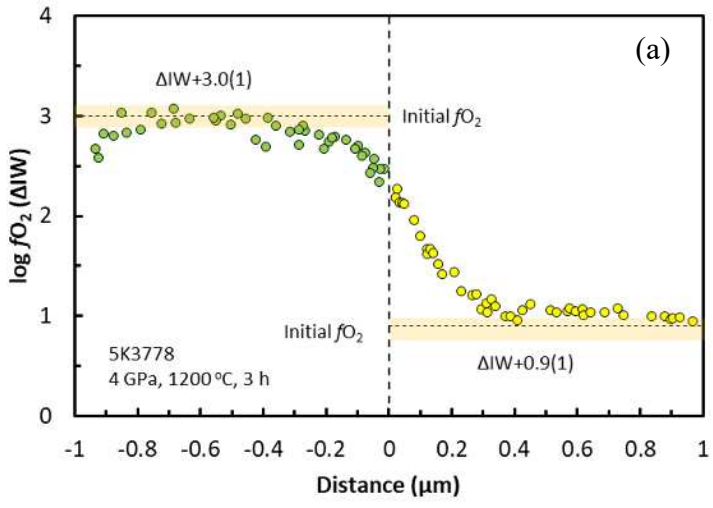

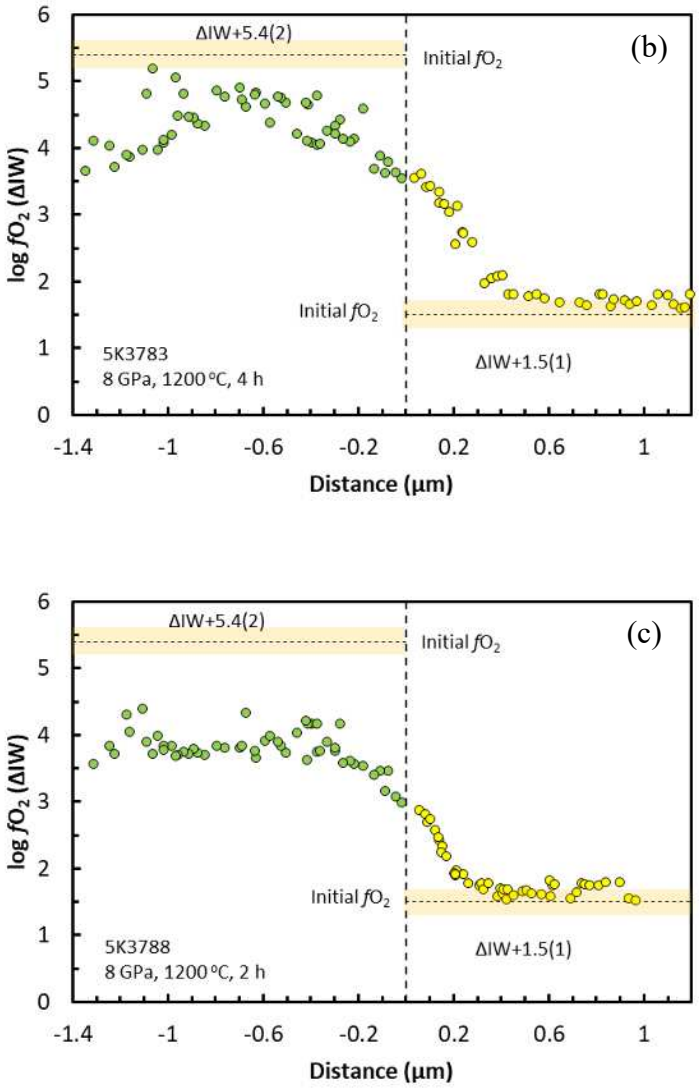

Fig. 5 Oxygen fugacity profile as a function of distance at different pressures and durations. Green dots are raw data in the original oxidized part of redox couple, while yellow ones are raw data in the original reduced part. Horizontal dashed line with yellow shaded region indicates the initial oxygen fugacity before redox experiment within standard deviation. Vertical dashed line is the initial contact interface.

4. Determination of diffusion coefficient

Along oxygen fugacity profile, fO_2 gradient leads to local re-equilibrium between Pt particle and surrounding olivine grains, which results in changing iron content in Pt alloy (X_{Fe}). As the amount of surrounding olivine grains is more than Pt alloy and Fe content in olivine is rather insensitive to fO_2, X_{Fe} is chosen to be the indicator of redox process. To determine diffusion coefficient, redox process in olivine aggregate is assumed to be one-dimension diffusion in semi-infinite space. Since X_{Fe} as a function of distance shows asymmetric feature (Fig. 6), Matano method was used to obtain diffusion coefficient (Matano, 1933). To get the robust fitting, largely deviated data were first removed to minimize possible interference. And the remaining raw data were fitted to the

BiDoseResp function as below,

$$C(x) = A_1 + (A_2 - A_1)[\frac{p}{1 + 10^{(Logx_1 - x)h_1}} + \frac{1-p}{1 + 10^{(Logx_2 - x)h_2}}] \quad , \tag{1}$$

where x is the distance of data points from the initial interface, $C(x)$ is the mole fraction of Fe in Pt alloy (X_{Fe}), others are fitting parameters. Except run 5K3783 which shows an obvious kink at the interface, other two runs demonstrate a smoothly fitted lines. Then position of Matano interface x was determined where the integration of x over the minimum (C_1) and maximum concentration (C_2) equals to each other, i.e.,

$$\int_{C_1}^{C_2} x dC = 0 \quad . \tag{2}$$

Pseudo-Matano interface was used for runs diffuse out at 8 GPa, which is meaningless physically except for getting diffusion coefficient in the next step. Iron-content dependent diffusion coefficient D was calculated according to the equation below,

$$D = -\frac{1}{2t}(\frac{dx}{dC}) \int_{C_1}^{C_2} x dC \quad , \tag{3}$$

where C is the iron content calculated from fitting line at position x. Although diffusion coefficient in redox couples at 8 GPa suffers from diffusion out and significant oxygen fugacity drop which makes it false, diffusion coefficient in the reduced part is still robust and reliable since it is independent from the oxidized one. In this case, only diffusion coefficient at the reduced part is adopted.

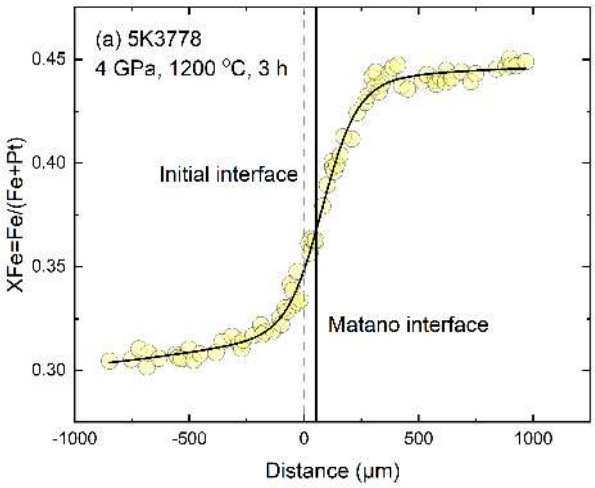

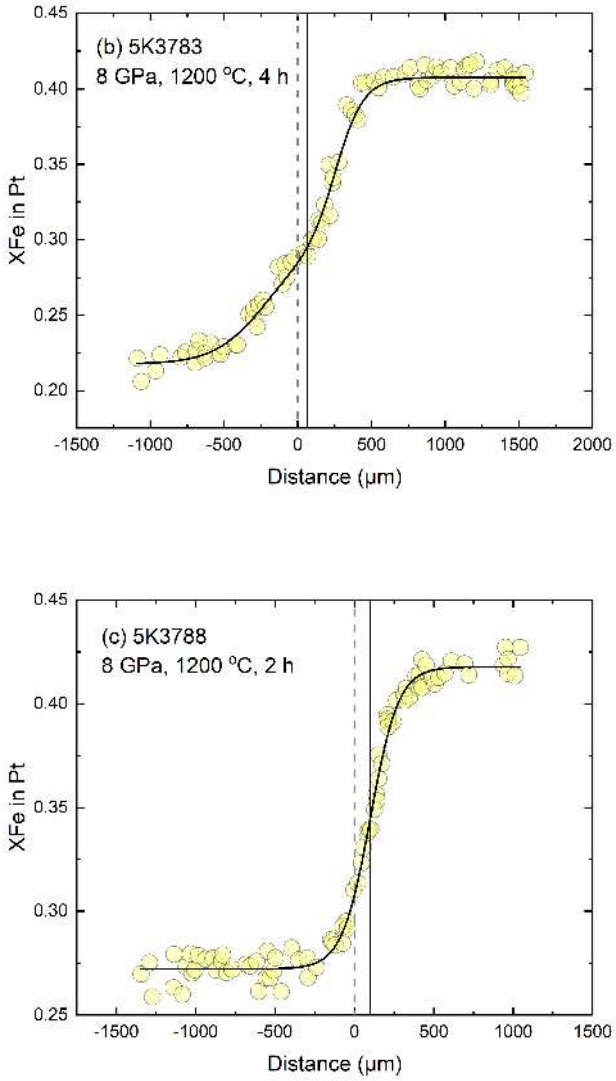

Fig. 6 Iron content in Pt alloy as a function of distance at different pressures and durations. The dashed vertical line is the initial contact interface, while the solid line is the (pseudo-) Matano interface. Diffusion profile at 4 GPa is complete, while profiles at 8 GPa diffuse out.

Results

Water content of redox couples from 4 to 8 GPa is within 30–180 wt. ppm (Fig. 3 and Table 3). Redox couples at 4 GPa suffers from water loss during redox experiment, while water content at 8 GPa before redox experiment is unknown. Within one redox couple, water content for the FMQ/RRO buffered part (hereafter named the oxidized part) is usually higher than that of the IW buffered part (hereafter named the reduced part).

Grain size of olivine in oxidized part before redox experiment is around 5–6.5 μm, and that in reduced part is around 1.5–3.5 μm (Table 1). After redox experiment, 10–60 % grain growth occurs. For the oxidized part, the grain size is around 9 – 12 μm, and for the reduced part, around 5-8 μm (Table 2). Since redox couple at 12 GPa is loosely sintered after redox experiment, its grain contrast

as well as oxygen fugacity profile is absent due to technical difficulty. Grain boundary for olivine grain at higher pressures is more obvious than that at 4 GPa, especially in the oxidized part (Fig. 4).

Oxygen fugacity profile as a function of distance from the initial contact interface at 4 GPa demonstrates asymmetric diffusion feature, while that at 8 GPa shows diffusing out feature or systematical drop of oxygen fugacity in the oxidized part (Fig. 5). In X_{Fe} profile, superfluous scattered data points were screened to ensure better fitting and thus more robust diffusion coefficient. At 4 GPa, X_{Fe} first increases gently over a long distance in the oxidized part, then increases rapidly until it levels out in the reduced part at the right side (Fig. 6a). At 8 GPa, X_{Fe} deviates from the initial X_{Fe} a little bit in the end of the left side which may result from too long run duration or too much water for run 5K3783 and 5K3788 respectively (Figs. 6b and 6c). However, both of them demonstrate a well-sustained diffusion profile in the reduced part, with X_{Fe} levels out in the end of the right side. The Matano interface shifted to the reduced part at 4 GPa, indicating relatively slower diffusion coefficient there. Since the initial X_{Fe} in the oxidized part is not maintained at 8 GPa, the Matano interface is pseudo one which is meaningless physically.

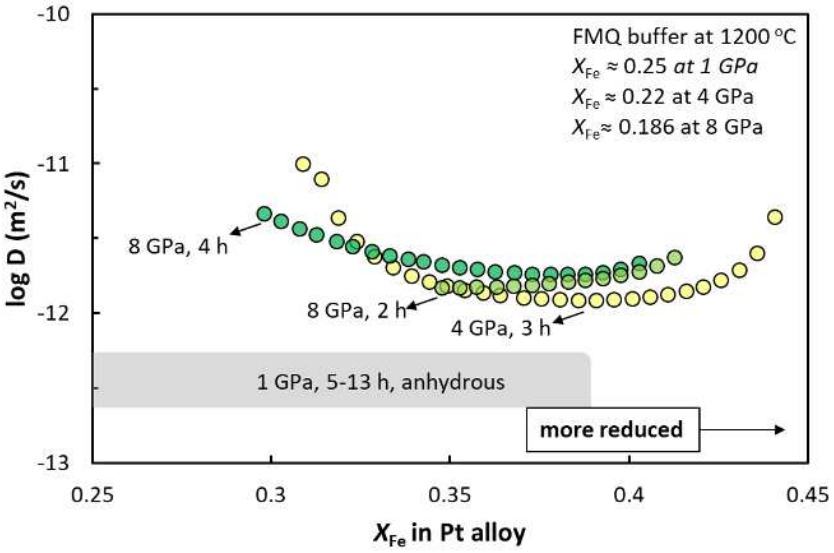

Fig. 7 Diffusion coefficient as a function of iron content in Pt alloy (X_{Fe}). Yellow and green points are diffusion coefficient at 4 and 8 GPa respectively. Light and dark green points are diffusion coefficient at 8 GPa for different durations. The grey shaded region is diffusion coefficient of dry reduced olivine at 1 GPa and 1200 °C for different durations. Oxygen fugacity of all the data is within IW and FMQ buffered condition.

Diffusion coefficient obtained versus X_{Fe} shows that diffusion coefficient increases with increasing pressure and water content (Fig. 7). Diffusion coefficient at 12 GPa is not available due to loosely sintered redox couple after recovery. In general, diffusion coefficient at 4 GPa is significantly higher than that at 1 GPa, which maybe due to the combined effect of pressure and water. The water influence on diffusion coefficient is negligible small at 4 GPa, i.e. 20 wt. ppm

water content different results in 0.1 log unit difference in diffusion coefficient (Table 2). Diffusion coefficient at 8 GPa seems to be a little higher than that at 4 GPa at the first glance (Fig. 7). However, when water content is the same (50 wt. ppm), they give the same diffusion coefficient (Table 2). At 8 GPa, the redox couple with slightly higher water contents by 20 wt. ppm exhibits a little bit faster diffusion coefficient (Fig. 8 and Table 2). Therefore, it is obvious that pressure has no influence on diffusion coefficient and thus redox kinetics, while water does have some, though may be not significant.

Extrapolating high pressure data to low pressure gives diffusion coefficient on the order of $10^{-11.9}$ m^2/s at 1 GPa (Fig. 8). Combined with diffusion coefficient of dry olivine at 1 GPa, it indicates that small amount of water can facilitate redox process in olivine by 0.5 log unit when oxygen fugacity is below FMQ buffer. The relationship between diffusion coefficient and water content is depicted in Fig. 9. Diffusion coefficient is enhanced by increasing water content, but the accelerate rate is diminishing. It shows that about 100 wt. ppm water can increase diffusion coefficient by about 1 log unit, and 2000 wt. ppm by about 2 log units when water content in olivine reaches the water solubility at the deep upper mantle according to the fitting equation. For the oxidized part in run 5K3788 whose oxygen fugacity dropped by about 1.7 log unit (Fig. 5c), its diffusion coefficient is expected to be $10^{-11.2}$ m^2/s according to the water content (Fig. 9 and Table 2), which is about 0.5 log unit faster compared with the apparent diffusion coefficient deduced from the final diffusion profile. Therefore, it is probable that the redox process first take place at the contact interface, when the initial oxygen reservoir runs out, the distant end far from the contact interface serves as oxygen source to provide redox component until the new oxygen fugacity level approaches the diffusion profile, which results in shortened apparent diffusion length and slowed apparent diffusion coefficient.

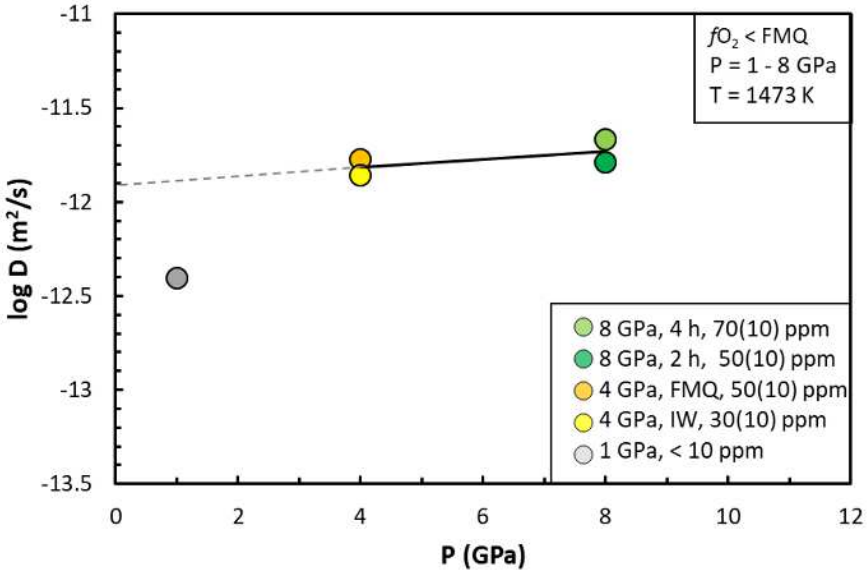

Fig. 8 Diffusion coefficient as a function of pressure and water content at 1200 ºC. Grey filled circle is from dry reduced part in redox couple at 1 GPa (Zhao et al., 2022). Yellow filled circles are from

4 GPa with different water contents, of which dark yellow represents the initially FMQ buffered part (⊿FMQ-1.5) and light one represents the initially IW buffered part (ΔIW+0.9) in the same run. Green filled circles are from 8 GPa with different water contents and durations, both of which represent the IW buffered part (ΔIW+1.5).

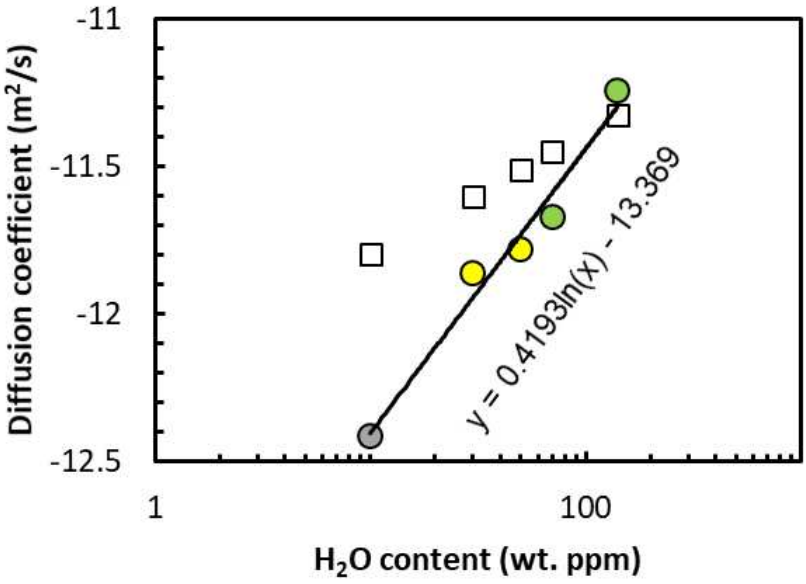

Fig. 9 Relationship between diffusion coefficient and water content from 1 to 8 GPa. Grey filled circle represents diffusion coefficient of dry olivine at 1 GPa whose water content is assumed to be 10 wt. ppm (Zhao et al., 2022). Yellow filled circles are diffusion coefficients of hydrous olivine at 4 GPa, and green ones are those of hydrous olivine at 8 GPa. Note that sample with the highest water content in run 5K3783 should have higher diffusion coefficient than demonstrated here since this value is derived from the profile diffusing out. Fitting line is shown below the data points. Grey filled cubes are diffusion coefficient calculated using H-D exchange data from Sun et al. (2019).

Discussion

Mechanism of redox kinetics for wet olivine

Diffusion coefficient of wet olivine at high pressure is 0.5–0.7 log unit faster than that of dry olivine at low pressure. Pressure is shown to have no influence on diffusion coefficient, therefore, the increased redox kinetics could be caused by mechanism whose diffuses faster than oxygen grain boundary diffusion. Since there is no cracks during redox experiment, high oxygen grain boundary caused by cracks and other short circuits could not be the dominant mechanism. Hydrogen is the most probable candidate. Diffusion coefficients obtained in this study lie on extended line of hydrogen diffusion associated with Mg site (Fig. 10). Furthermore, diffusion coefficient calculated using H-D exchange experiment matches diffusion coefficient in this study well, whose value is within 5% of ours (Fig. 9).

When slab subducts into the upper mantle, oxygen budget within slab evolved according to the

evolution of its water content. Regions with no or small amount of water cannot release oxygen budget fast, but to preserve until it reaches deep mantle. However, regions with high water content can reach new oxygen equilibrium quickly and release oxidizing component. When water content in the surrounding reduced mantle is lower than the slab, there will be redundant oxidizer wander around. Otherwise, the surrounding mantle will be oxidized more quickly. However, even assuming the maximum water content in olivine (2000 wt. ppm), the slab can only be altered by ~30%, in the absence of fluid.

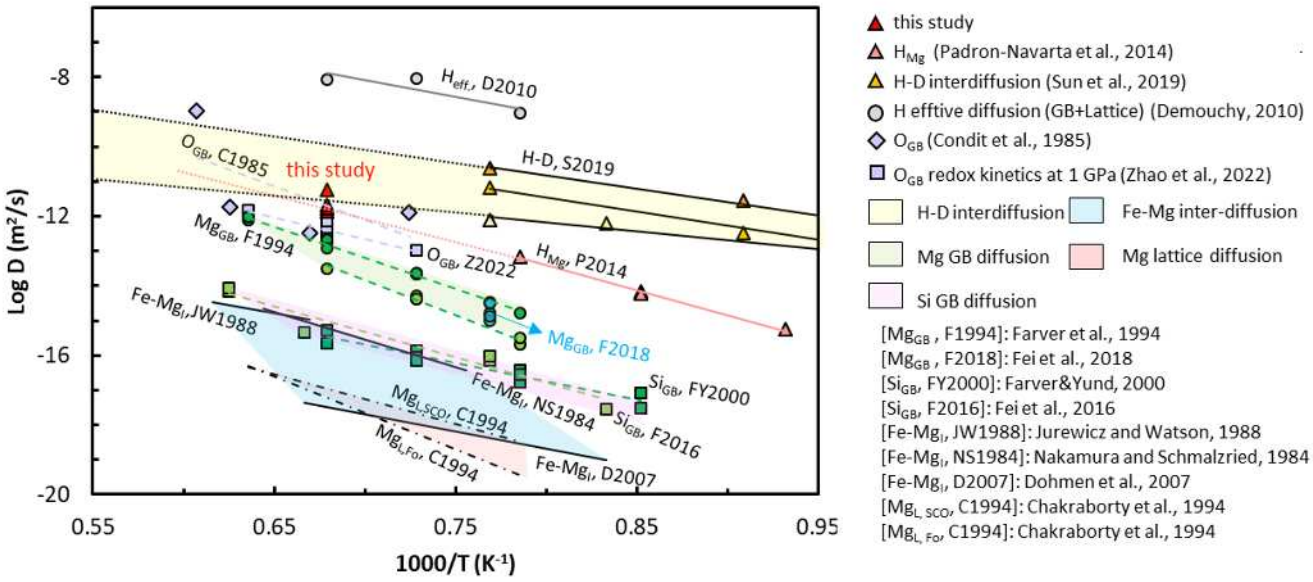

Fig. 10 Diffusion coefficient in wet olivine at high pressure compared with diffusivities of other elements in olivine.